Determination of vectors' reproduction spots in Makkah using GIS and remote sensing techniques

Waleed Abou El-Saoud, Safwat S. Gabr, Ibrahim H Abdel-Rahim, Essam Morsy
The Custodian of the Two Holy Mosques Institute of Hajj and Umrah Research, Umm Al-Qura University

Abstract

The Holy City of Makkah receives millions of pilgrims every year. The natural environment in the adjacent areas of Makkah is a suitable environment for the growth of many vectors. This environment is characterized by high temperature, high humidity, and is usually located away from direct air currents, a good environment for the growth of such vectors. Recent statistics from the World Health Organization (WHO) indicate that vector-borne diseases account for 17% of all infectious diseases worldwide. The Kingdom of Saudi Arabia is exerting great efforts and developing intensive programs to control the spreading of these vectors to maintain a healthy community, mainly for pilgrims. Early detection of the growth locations of these vectors and determining their spreading patterns is very important for its control. The main aim of this study is to identify the high-risk zones of the vectors using remote sensing and GIS through modeling and analyzing the available climatic, rainfall, wind, land surface temperature (LST), normalized vegetation index (NDVI), temperature, and population density data to identify the most critical areas in Makkah for vector growth. The primary results from this study indicate that the areas with high population density, a relatively low topography, and a high surface temperature (ranges between 25-35 °C) are the most suitable areas for vectors growth and/or spreading. No significant impact of the NDVI on the presence of these vectors. The study also showed that the most susceptible areas to vectors growth in Makkah are; Al-Zhra, Hendawyiah, Khadyiah, Masfalah, Utabyiah, Hegon, and Tandbawy respectively, and some locations in Al-Awalyi & Waly El-Ahad planned districts. Accordingly, the study recommends the need to rely on satellite imagery and geographic information systems in vector control programs to identify areas vulnerable to vectors reproduction.

1. Introduction:

Worldwide, there are about three hundred species of mosquitoes, which transmit several infectious diseases to humans and animals. *Culex*, *Anopheles* and *Aedes* are the most common species. *Aedes albopictus* is known as Asian tiger mosquito. *Aedes agypti* is known as yellow fever mosquito and it transmit also dengue fever virus. Table 1 shows infectious diseases transmitted by various species of mosquitoes [1].

Table 1: Infectious diseases transmitted by various species of mosquitoes [1].

Vectors (Mosquitoes)	**Infectious Diseases**
Anopheles	Malaria, Lymphatic filariasis
Culex	Lymphatic filariasis, Japanese encephalitis, Other viral diseases
Aedes	Yellow fever, dengue fever, dengue haemorrhagic fever, other viral diseases and Lymphatic filariasis
Mansonia	Lymphatic filariasis

The female of *Aedes aegypti* (*Ae. Aegypti*) is considered the principal vector of dengue fever [2]. *Ae. aegypti* is a peridomestic mosquito which lives around human dwellings, it is active during the day time, mainly consumes human blood, and goes through a complete life cycle (from egg stage to larval and to adulthood stage). Meteorological parameters such as air temperature play a vital role in controlling the various life stages *Ae. Aegypti* [3]. The Aedes mosquitoes have four life stages: eggs, larva, pupa and adult. Mosquitoes can life and reproduce inside and outside the home. The entire life cycle, from egg to an adult, takes approximately 8-10 days. Larvae are aquatic and develop into pupae in as little as five days (Figure 1) [4].

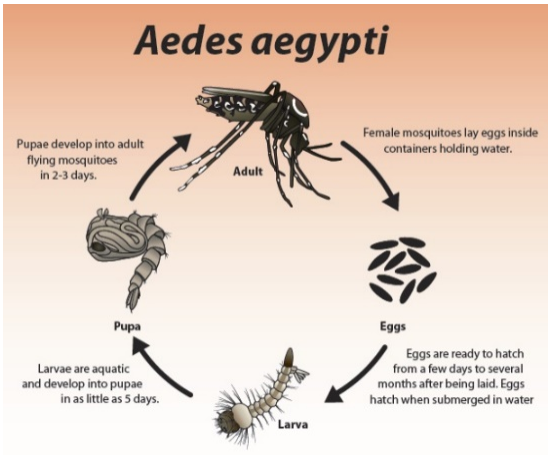

Figure 1. Life cycle of Aedes Aegypti, [4].

The close association of the vector of dengue viruses (*Ae. Aegypti*) with humans and the environment allows this mosquito species to persist in regions that may otherwise be non-suitable depending on the climatic variables alone [5]. The relationship between the *Ae. aegypti* flight performance and the temperature as well as relative humidity was studied by [6]. Generally, below 27°C, the flight performance was greater. Best flight performance was demonstrated at 21°C temperature, however the temperature ranged from 15 to 32°C at which the mosquitos were able to fly. In concerning to the relative humidity, mosquitos' flight was not affected within 30 to 90 % relative humidity range, regardless of the air temperature, except at 32°C, where 30 % relative humidity had a significant effect on mosquitos' flight. Several researchers [7] determined the development, growth, and survival of *Ae. aegypti* at several temperature levels ranging from 15 to 34^{o}C. The results indicated that survival of adult mosquitos was low at 15°C temperature and 3% relative humidity, better at 27°C (90%) and highest at 20 °C (92%).

Geographic information systems (GIS), global positioning systems (GPS), remote sensing, and spatial statistics are tools to analyze and integrate the spatial component in epidemiology of vector-borne disease into research, surveillance, and control programs based on a landscape ecology approach [8]. Over the past twenty-five years, the use of remote sensing techniques for mapping of the vector-borne infectious diseases has evolved significantly. Worldwide, epidemiologists are used the new remote sensing techniques to study the epidemiology of a variety of insects-borne diseases [9].

Multispectral satellite data can be used to predict arthropod-borne disease trouble spots. This is dependent on clear understandings of environmental factors that determine the presence of disease vectors [10]. Several health studies and researches have used remotely sensed data for monitoring, surveillance, or risk mapping, particularly of vector-borne diseases [11]. Vector habitats were identified and characterized through using of the association between satellite-derived environmental changes such as temperature, humidity, and land cover types and vector density [9].

In Southern Chiapas, Mexico, remote sensing was used as a landscape epidemiologic tool for identification villages at high risk for malaria transmission, as defined by adult *Anopheles albimanus* abundance [12].

In the Republic of Korea, it was suggested that the classified remotely sensed data could potentially be used to estimate the distributions of larval and adult mosquito populations [13].

In African highlands, landuse change has been hypothesized to be one of the mechanisms for malaria epidemics because it can alter the physical and chemical characteristics of mosquito breeding habitats [14].

In western Kenya highlands, it was shown that one meter spatial IKONOS images combined with computer modelling based on topographic land-cover features were useful tools for demonstration of the larval habitat of the anopheles mosquitos, which could assist to control of malaria spreading [15]. Also, In Kenya, Rift Valley fever viral activity was detected by satellite remote sensing imagery [16].

In Jeddah, Saudi Arabia, geographical information system (GIS) was applied to analyze the presence of dengue fever in various seasons of the year. It was shown that the central areas in Jeddah are the main hotspots for dengue fever; however, its intensity varied both in space and time [17].

It was shown that the Geographic Information Systems, combined with remote sensing analysis, have the potential to assist in minimizing disease risk. Examples are used from subtropical Queensland, Australia, where the salt marsh mosquito, *Aedes vigilax*, and the freshwater species, *Culex annulirostris*, are vectors of human arbovirus diseases such as Ross River and Barmah Forest virus disease. *Culex annulirostris* is also implicated in the transmission of Japanese Encephalitis. Mapping the breeding habitats of the species facilitates assessment of the risk of contracting the diseases and also assists in control of the vectors [18].

Other Researchers [19] applied the global environmental data for mapping infectious diseases distribution. Others [20] had seen great potential for the use of new technologies and approaches, such as GIS and decision support systems for the predication, prevention and control of the vector-borne and other infectious diseases.

The aim of the current study is; (1) to identify the environmental factors, which contributes to vector reproduction using Landsat 8 data analysis, (2) to correlate the extracted factors with vector occurrence pattern from the data collected from the municipality of Makkah reports (from 2013-2017), and (3) to predict potential high-risk zones for a vector reproduction.

2. Materials and Methods:

2.1. Study Area. This ecological study was conducted in the city of Makkah districts, western region of kingdom of Saudi Arabia. Makkah occupies a total area of 1200 km², 105,037 km^2 of which 7 million inhabitants occupies, 2016 [21]. Situated at altitudes ranging from 277 to 350 meters, Makkah is open for visitors from the entire world, particularly during the religious occasions of Hajj and Umrah. The total number of Muslims who visited the holy city of Makkah for Hajj during 2016 was 1.862.909 [21]. This mass gathering in a small spatial region during a short period of time represent a big challenge to the country.

In the current study, Landsat 8 data acquired in October 29, 2016 (after the rainfall event of October, 24) as well as the SRTM digital elevation model have been analyzed using ERDAS imaging 2016 software package. ArcGIS 10.4 is used for GIS spatial and geostatistical analysis of the data as well as map production.

2.2. larvae vectors. eggs foci data reported and collected in ovitraps from 2013 to 2016 were used in this study. The data was obtained from the municipality vector reporting system, which contains the address for each larva focus and ovitrap and the dates of the survey. The collected data contains larvae known to be harmful; *Aedes agypti*, *Culex antennatus*, *Culex pipiens*, *Culex quinquefasciatus*, *Culex tritaeniorhynchus*, *Culex zombaensis* and other unharmful larvae (Figure 2).

2.3. Climatic Data. Generally, climate of Makkah district can be described as arid weather during the year. Hajj Research Institute (HRI) has its meteorological monitoring network, which consists of eight meteorological monitoring stations are distributed allover Makkah. The data are gathered and analyzed for the 2016, to get the updated image about the weather conditions of Makkah districts. The discussed meteorological parameters for the study area can be summarized as following:

2.3.1. Temperature.

The temperature of Makkah district ranges between 14.99 to 47.66 °C all over the year, where the western and southeastern regions of Makkah is characterized by high temperature compared with the central region (Figure 3).

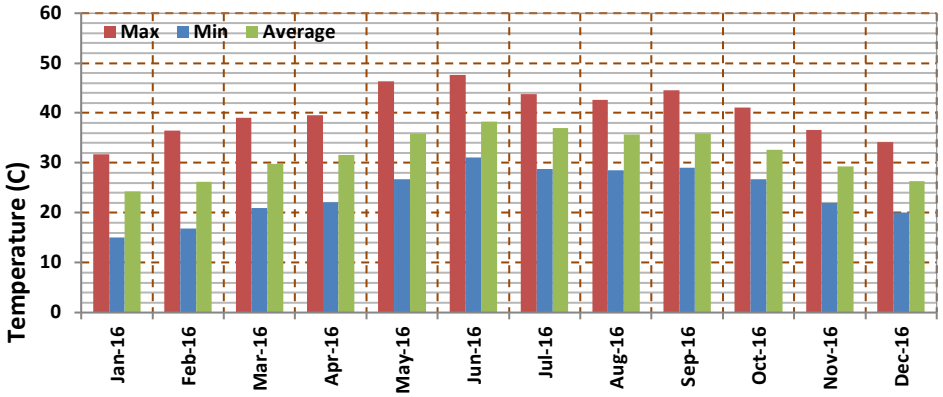

Figure 3: Average monthly variation of temperature in Makkah during 2016 (Kudy).

2.3.2. Relative Humidity.

The spatial distribution of relative humidity is shown on (Figure 4), where the central region of Makkah was characterized by low relative humidity (35%) and increased gradually in the directions of eastern and western regions of Makkah. Generally, the relative humidity ranged between 35-41% allover Makkah, whereas in the month of November, the range lying between 10.34 to 75.19%.

2.3.3. Rainfall

The complexity in the topography was reflected clearly on the spatial distribution of rainfall in Makkah (Figure 5), where the central region of Makkah was characterized by high rainfall compared with the north and southwest regions of Makkah. Generally, the rainfall ranged between 21.59-86.61 mm allover Makkah.

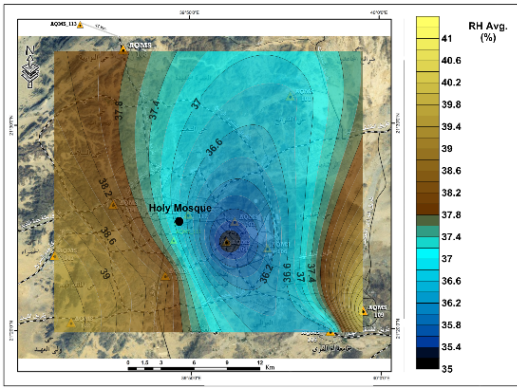

Figure 4: Contour map of relative humidity (%) in Makkah during 2016.

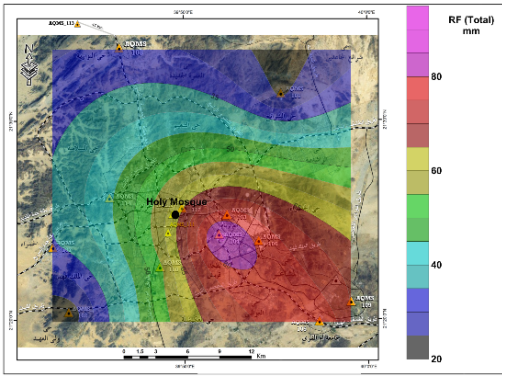

Figure 5: Contour map of rainfall (mm) in Makkah during 2016.

According to the World Health Organization (WHO) the interactions between temperature and rainfall are important as determinants in a dengue transmission, as cooler temperatures affect the survival of adult mosquitoes, thus influencing transmission rates [22]. Furthermore, rainfall and temperature may affect patterns of mosquitoes feeding and reproduction, and hence the population density of vector mosquitoes.

2.4. Spatial Diffusion Pattern

All reported locations of larvae foci building and the locations of the ovitraps were geocoded using the location addresses. Spatial statistical techniques used in this study included Kernel's density in order to determine the dens and specific patterns of distribution on the study area in square kilometers.

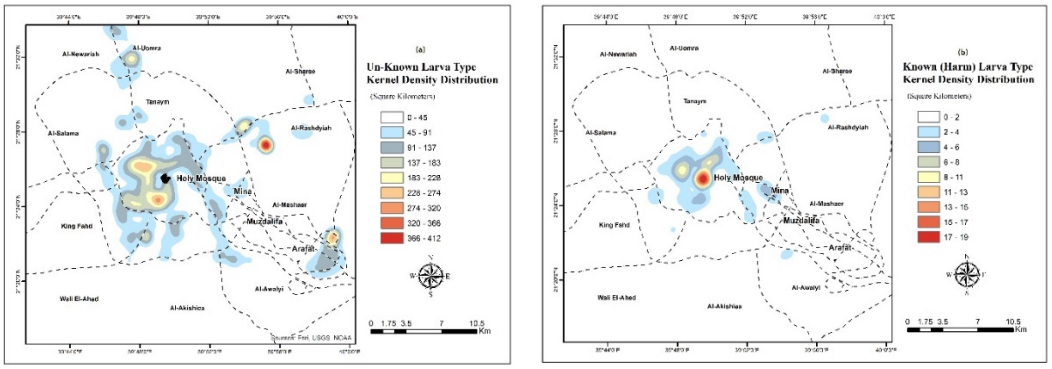

Figure 2. Spatial distribution of (a) the unharmful larva (b) the harmful larva in the study area.

2.5. Environmental parameters affecting Vectors' reproduction:

The major phase of the data collection was to identify the environmental factors, which had significantly influenced the larva distribution pattern. All the environmental data was collected from remote sensing data; this technique has been tested successfully by [23]. Four environmental parameters were extracted from Landsat 8 data (landuse, NDVI of vegetated and non-vegetated areas, land surface temperature, LST) in addition to the population density.

2.5.1. Image Classification (Land use / land cover map):

Image classification is the process of assigning land cover classes to pixels, Landsat 8 Operational Land Imager (OLI) imagery of Makkah using the Maximum Likelihood Classification tools.

Six classes were established as mountains, green areas and water bodies, Urban areas, Wadis, construction areas, and open (cleared) areas. Descriptions of these land cover classes are presented in (Table 2).

Table 2: Land cover classification scheme.

Mountain	Hill, large rock, rugged terrain
Urban Area	Residential, commercial services, industrial, mixed urban or built-up land
Green Area-Water Body	Trees, agriculture area, vegetated area, water body
Wadis	Soil types related to Wadi deposits and sand dunes
Construction Area	New areas undergoing planning for future development
Open (cleared) class	Bare soil, sandy soil, desert, open land

2.5.2. Calculation of Land Surface Temperature (LST) and Normal Difference Vegetation Index (NDVI):

Land surface temperature (LST) is defined as the temperature felt when the land surface is touched with the hands or the skin temperature of the ground [24]. As one of the most important aspects of the land surface, LST has been a main topic for developing methodologies to be measured from space. Calculating LST from remote sensed images is needed since it is an important factor controlling most physical, chemical, and biological processes of the Earth [25]. There is a growing awareness among environmental scientists that remote sensing can play a role in providing the data needed to assess ecosystems conditions and to monitor change at all special scales [26].

In the present study, the Land Surface Temperature (LST) and NDVI can be retrieved from Landsat 8 satellite image following the steps of (Figure 3), where the Thermal Infrared Sensor (TIRS) band 10 was used to estimate brightness temperature and bands 4 and 5 were used for calculating the NDVI. The metadata of the satellite images used in the algorithm is presented in (Table 3).

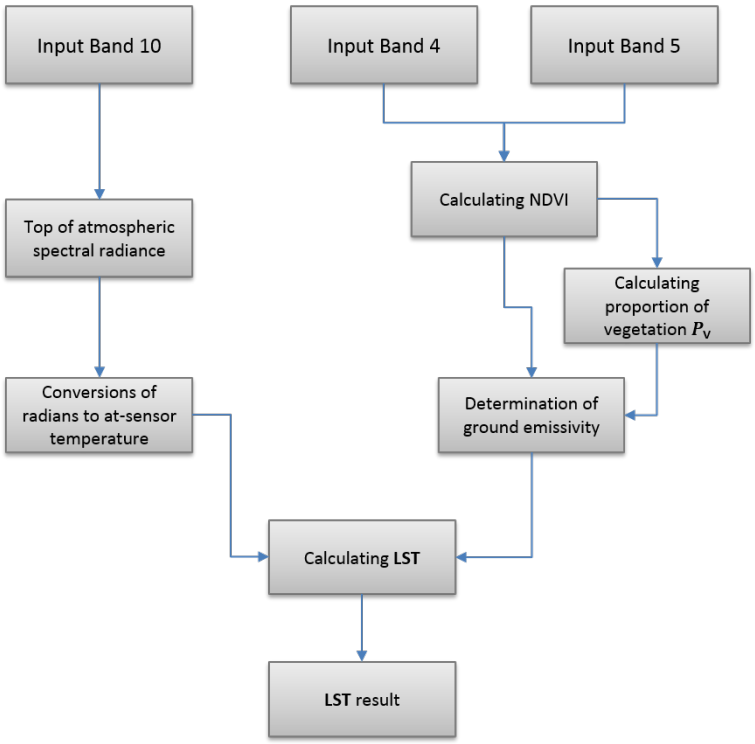

Figure 3: Flowchart for LST retrieval

Table 3: Metadata of the Landsat 8 satellite image.

Thermal constant, Band 10	
K1	774.8853
K2	1321.0789
Rescaling factor, Band 10	
M_L	0.000342
A_L	0.29
Correction, Band 10	
O_i	0.29

2.5.2.1. Top of Atmospheric Spectral Radiance:

Landsat 8 consist of quantized and calibrated scaled Digital Numbers (DN) representing multispectral image data acquired by both the Operational Land Imager (OLI) and Thermal Infrared Sensor (TIRS). The products are delivered in 16-bit unsigned integer format and

can be rescaled to the Top of Atmosphere (TOA) reflectance and/or radiance using radiometric rescaling coefficients provided in the product metadata file.

The first step of the algorithm is converted the TIRS bands data to the TOA spectral radiance (L_λ) using the formulas taken from the USGS webpage [27]:

$$L_\lambda = M_L * Q_{\text{cal}} + A_L$$

Where;
L_λ = TOA spectral radiance (Watts/ (m2 * srad * μm))
M_L= Band-specific multiplicative rescaling factor from the metadata (RADIANCE_MULT_BAND_x, where x is the band number)
A_L = Band-specific additive rescaling factor from the metadata (RADIANCE_ADD_BAND_x, where x is the band number)
Q_{cal}= Quantized and calibrated standard product pixel values (DN)

2.5.2.2. Conversion of Radiance to At-Satellite Brightness Temperature:

After the digital numbers (DN_s) are converted to radiance, the TIRS band data should be converted from spectral radiance to brightness temperature (BT) using the thermal constants provided in the metadata file. The following equation is used in the tool's algorithm to convert radiance to BT [27]:

$$BT = \frac{K_2}{\ln[(K_1 / L_\lambda) + 1]} - 273.15$$

Where;
BT = At-satellite brightness temperature (K)
L_λ = TOA spectral radiance (Watts/(m2 * srad * μm))
K_1 = Band-specific thermal conversion constant from the metadata (K1_CONSTANT_BAND_x, where x is the thermal band number)
K_2 = Band-specific thermal conversion constant from the metadata (K2_CONSTANT_BAND_x, where x is the thermal band number)

For obtaining the results in Celsius, the radiant temperature is revised by adding the absolute zero (approx. −273.15°C) [28].

2.5.2.3. Calculate the Normal Difference Vegetation Index (NDVI):

Landsat visible and near-infrared bands were used for calculating the Normal Difference Vegetation Index (NDVI). The importance of estimating the NDVI is essential since the amount of vegetation can be used as a factor for vectors distribution. The calculation of the NDVI is important because, afterward, the proportion of the vegetation (P_V) should be calculated, and they are highly related with the NDVI, and emissivity (ε) should be calculated, which is related to the P_V:

$$NDVI = NIR(band\ 5) - R(band\ 4) \ / \ NIR(band\ 5) - R(band\ 4)$$

Where; NIR represents the near-infrared band (Band 5) and R represents the red band (Band 4).

2.5.2.4. Calculating the Proportion of Vegetation (P_V):

A method for calculating P_V suggests using the NDVI values for vegetation and soil ($NDVI_V$ = 0.5 and $NDVI_S$ = 0.2) to apply in global conditions [29]:

$$Pv = (NDVI - NDVIs \,/\, NDVIv - NDVIs)2$$

Where; $NDVI_S$ and $NDVI_V$ Represent the minimum and maximum values of the NDVI image, respectively, which, provided that the area is large enough, will correspond with areas with no vegetation (bare soil) and with full vegetation coverage.

2.5.2.5. Calculating Land Surface Emissivity (LSE):

The land surface emissivity (LSE (ε)) must be known in order to estimate LST, since the LSE is a proportionality factor that scales blackbody radiance (Planck's law) to predict emitted radiance, and it is the efficiency of transmitting thermal energy across the surface into the atmosphere [30]. The determination of the ground emissivity is calculated conditionally as suggested in [29]:

$$\varepsilon_\lambda = \varepsilon_{V\lambda} P_V + \varepsilon_{s\lambda} (1 - P_V) + C_\lambda$$

Where; ε_V and ε_s are the vegetation and soil emissivity respectively, and C represents the surface roughness (C = 0 for homogenous and flat surfaces) taken as a constant value of 0.005 [31].

When the NDVI is less than 0, it is classified as water, values between 0 and 0.2, it is considered that the land is covered with soil or rocks, values between 0.2 and 0.5 are considered mixtures of soil and vegetation cover and is applied to retrieve the emissivity. In the last case, when the NDVI value is greater than 0.5, it is considered to be covered with vegetation, and the value of 0.973 is assigned. The last step of retrieving the LST or the emissivity corrected land surface temperature T_s is computed as follows [32]:

$$T_s = \frac{\mathrm{BT}}{\{1 + [(\lambda \mathrm{BT}/\rho) \ln \varepsilon_\lambda]\}},$$

Where; T_s is the LST in Celsius (◦C, (2)), BT is at-sensor BT (◦C), λ is the wavelength of emitted radiance (for which the peak response and the average of the limiting wavelength (λ = 10.895) [15] will be used), ε_λ is the emissivity calculated, and

$$\rho = h\frac{c}{\sigma} = 1.438 \times 10^{-2}\ \mathrm{m\ K},$$

Where; σ is the Boltzmann constant (1.38×10^{-23} J/K), h is Planck's constant (6.626×10^{-34} J s), and c is the velocity of light (2.998×10^{8} m/s) [33].

2.5.3 Population Density:

Population density in any urban area is another factor that has to be taken into account in preventing an outbreak of diseases. The data of population density for Makkah districts have been collected from the database of Makkah Region Development Authority and The Census data of the General Authority for Statistics (2010). In our study, we removed the mountainous areas from our calculation to better calculate the actual locations for population density. These locations have their own unique characteristics that are easily identifiable and can be located visually. Population data was also used to verify the result. A densely populated area stands a higher chance of experiencing a disease even if the mosquito house index in that area is low. This is because mosquitoes do not have to travel far to search for its victims. Therefore, an outbreak of infectious diseases can and will be able to spread rapidly in such an area.

3. Results and discussion:

This study found that areas at a high risk for vectors reproduction could be identified through the integration of environmental factors derived from remote sensing with other data from GIS analysis and modeling. The weighted overlay function was chosen to create the risk area map. The following sections provide a detailed analysis of the impact of each variable:

3.1. Land cover and land use classification

The land cover and land use information of Makkah districts obtained from the Landsat 8 image is highlighted in Figure 4. From the classification result, it was found that most larvae location found in urban areas, followed by horticulture areas especially at Arafat area. Just a few locations were reported in the construction areas. The reason why mosquito larvae location found mostly in urban areas can be explained by a number of factors. For an urban area, proper infrastructure such as a good drainage system is very important. A poor drainage system will create pools of stagnant water, which are suitable breeding grounds for mosquitoes. The same problem occurs in construction areas. In areas with a high population density, vector disease transmission can and will occur rapidly. Other areas that also have a record of larvae are areas that are not cleanly maintained, areas that have been left idle, areas with rapid development and areas having temporary structures.

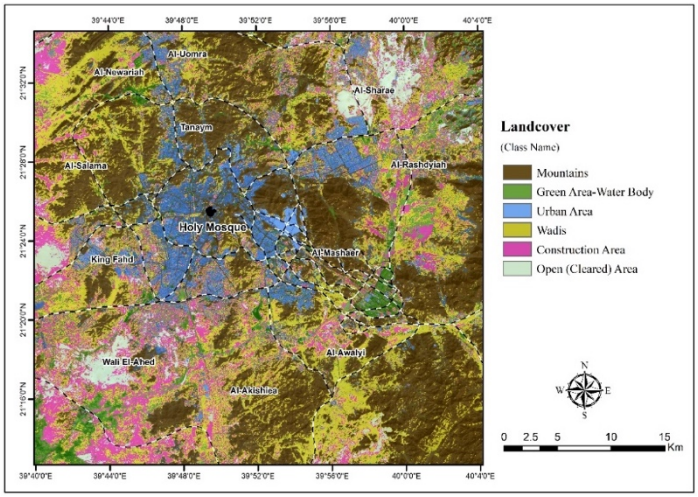

Figure 4. Unsupervised classification of the study area.

3.2. Land surface temperature (LST)

The temperature profile of the land surface over the study area is shown on the LST map in (Figure 5) which was derived from the Landsat-8 thermal infrared (TIRS) band. The areas with high levels of LST (in red) can be correlated to Wadies and construction areas, while the blue area equate to either an urban area or a vegetated area. The LST map shows that the temperature ranges from 23°C to 45.82°C. Most of the reported mosquito larvae occurred in the areas with a temperature range from between 25.0°C to 35.0°C. This temperature range is very conducive to the mosquito breeding cycle as an increase in the number of times that the mosquito breeds will also increase the likelihood of the emergence of the diseases outbreak.

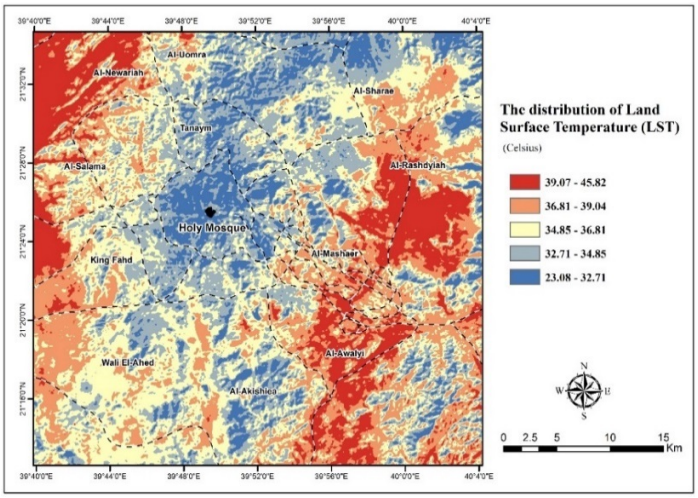

Figure 5. The distribution of Land Surface Temperature from Landsat 8 satellite image.

3.3. Normalised Difference Vegetation Index (NDVI):

NDVI is usually used to derive the vegetation index from satellite images. For this study, it was used to identify the green areas over the study area, in which; NDVI values range from −1 to +1, where negative values correspond to an absence of vegetation [34]. Figure 6 shows that the range of NDVI values in the study area is between -0.101 and 0.457. Built-up areas and other land use class are shown in white, while the dark colored (black) areas refer to the vegetation density of an area. This study found that the vegetation density of an area was not a major factor in influencing the number of mosquito larvae occurred.

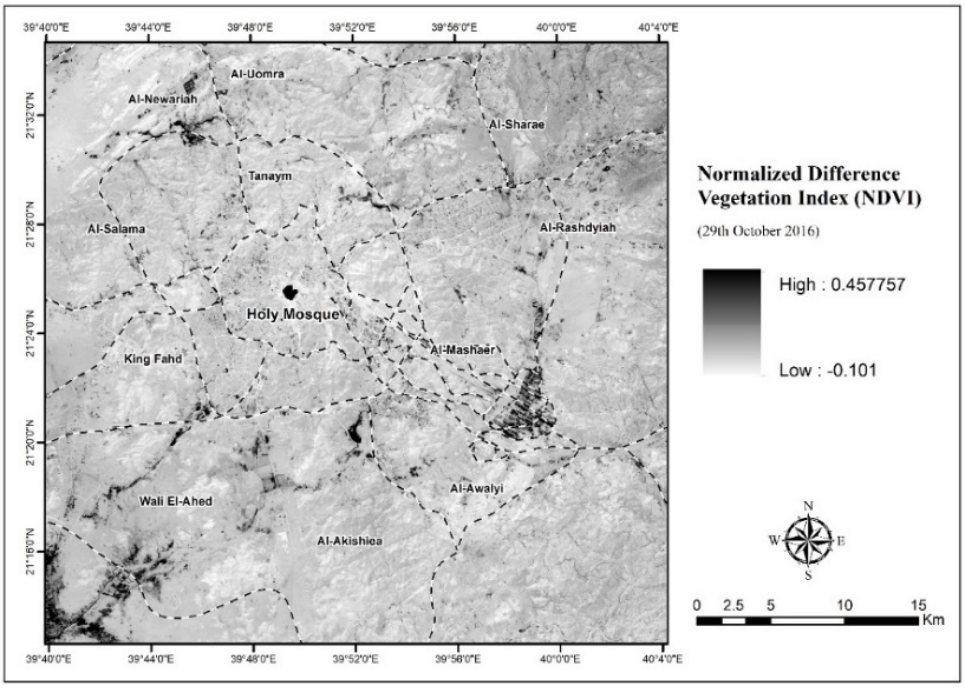

Figure 6. NDVI image of Makkah districts on 29th October 2016.

3.4. Population Density:

Using the data collected from Makkah Region Development Authority and The Census data of the General Authority for Statistics (2010), and by excluding the mountainous regions, the population density for each of Makkah districts can be summarized in (Figure 7). This figure show that most of the high density districts are located close to the Haram area. Al-Zahra, Hindawia, Khalidiya, Masfalah, Hujun, Otaibia, Khansa, Mabda, Al-Gamia, Al-Adel and Aziziah respectively.

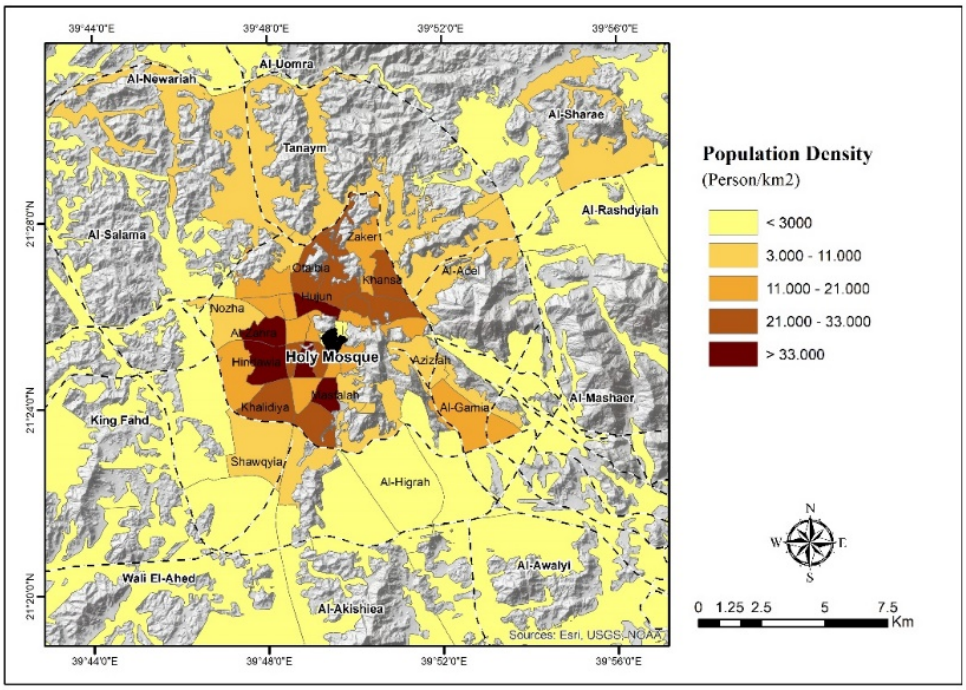

Figure 7. Population density map of Makkah district.

Identification of Vectors' Propagation Risk Areas in Makkah districts

Each of the four variables was tested using the weighted overlay function technique in the ArcGIS software. This technique is usually used for applying a common measurement scale of values to diverse and dissimilar inputs in order to create an integrated analysis in (Figure 8). The priority value was ranked as low, medium and high (1 to 3) for each variable. A low value means the sub variable had a low intensity influence; a medium value equated to a greater risk influence to the spreading and a high value equated to a very significant influence on the vectors spreading pattern. The detailed weighting values for all four environmental variables that were identified as an indicator factor of vectors spreading are presented in (Table 4). For the information obtained, the following algorithm was used to develop the vectors spreading zone from each environmental indicator as shown below.

(Land cover) + (Population Density) + (NDVI) + (LST)

Identification of areas with a high risk of having a disease outbreak requires the input of the above stated parameters for this analysis. The analysis results of the parameters were then given a specific priority value based on the requirements of this study. The priority values were ranked as 'low', 'medium" and 'high'. The contribution of these values in every spatial

layer were given a value between 1 (low) to 3 (high), where a value of 1 means a very low contribution while a value of 3 means a high contribution to a disease outbreak. Areas with the highest score can then be identified as being areas with a very high risk of having a disease outbreak.

The potentially high-risk areas for the occurrence of a disease incidences over the study area are shown in (Figure 9), which is concentrated mainly within; Al-Zhra, Al-Hendawyiah, Al-Khadyiah, Al-Masfalah, Al-Utabyiah, Al-Hegon, Al-Tandbawy, Al-Maabd, Al-Andlus and some locations in Al-Awalyi & Waly El-Ahad planned districts. Reported larva data obtained from the municipality vector reporting system was used to verify the above result.

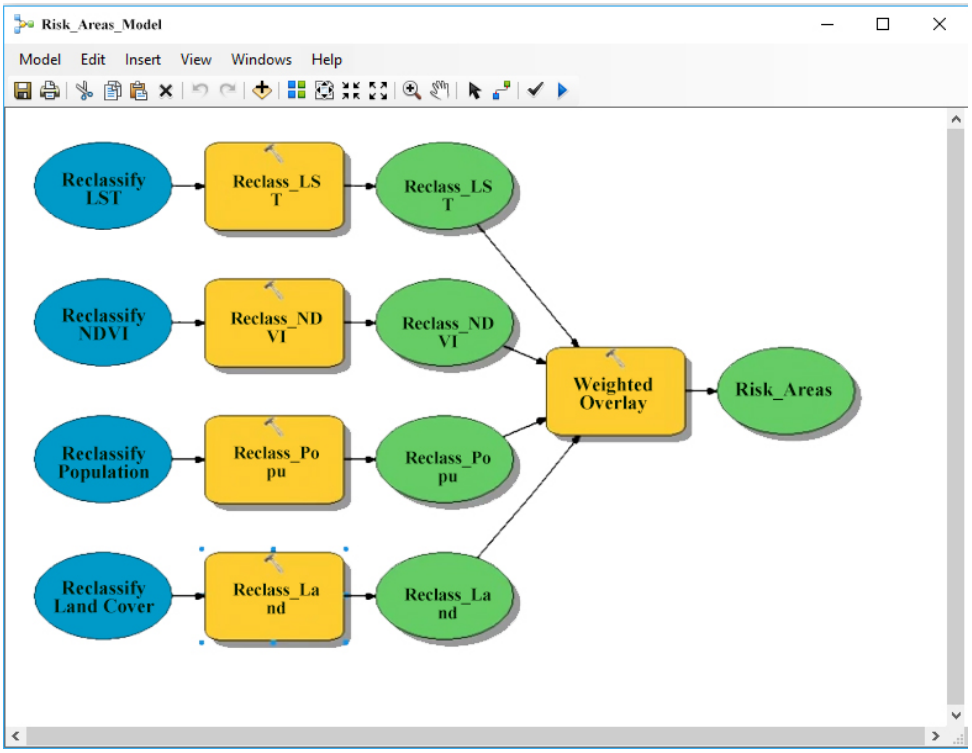

Figure 8. A model workflow for locating of the areas which are likely to be affected by vector reproduction.

Table 4. The weighted overlay value for environmental risk indicator.

No.	Environmental Factors		Risk Value
	Raster	Field	
1	Land Cover	Mountain	1
		Green Area-Water Body	2
		Urban Area	3
		Wadis	1
		Construction Area	3
		Open (Cleared) Area	1
2	NDVI	Vegetation area	2
		Non-vegetation area	1
3	LST	Low	3
		Medium	2
		High	1
4	Population density	Very low	1
		Low	1
		Medium	2
		High	3
		Very high	3

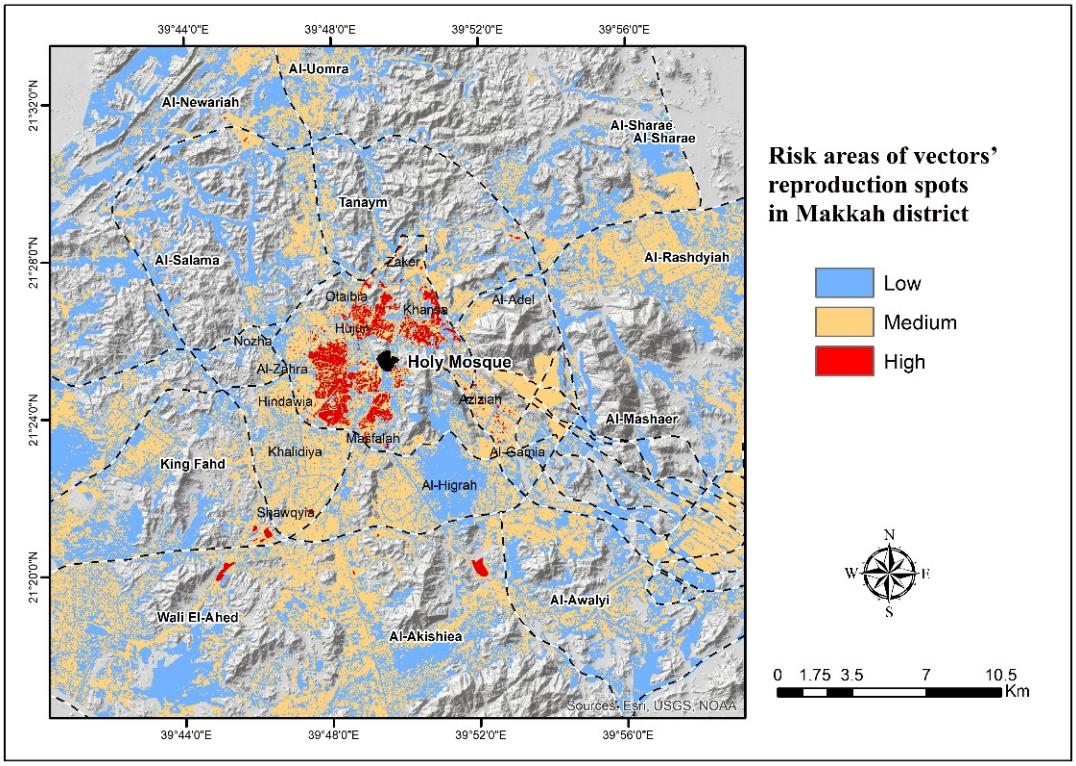

Figure 9. Risk areas of vectors' reproduction in Makkah districts.

4. Conclusions

Remote sensing satellite data such as Landsat 8 is capable of providing information on the environmental factors: land cover/use, land surface temperature (LST), NDVI and topography, which are influential to a vectors' reproduction. The high-risk areas for a larva occurrence are significantly correlated with environmental factors obtained from remote sensing data, which are then integrated with rainfall, temperature, humidity and population density data. The present study showed the main factors suitable for larva locations. These locations are mostly of densely population, near construction sites, have a low land topographically with surrounding high values of land surface temperature (LST). Such areas represent an ideal habitat area types may affect by epidemic outbreak after days of heavy rainfall followed by high temperature. Results from this research indicate that the identified 'high risk' areas are located within Al-Zhra, Al-Hendawyiah, Al-Khadyiah, Al-Masfalah, Al-Utabyiah, Al-Hegon, Al-Tandbawy, Al-Maabd, Al-Andlus and some locations in Al-Awalyi & Waly El-Ahad planned districts. The result also shows a strong correlation between locations of reported harm locations with the potential high-risk area map, which was created based on environmental factors used to identify the risk areas. Remote sensing and GIS technologies are important tools for the effective surveillance and prediction of the vector born disease in order to reduce the number of outbreak cases. GIS analysis has the ability to model a risk map of vector born disease distribution through the use of the weighted overlay function, which enabled the users to easily identify high risk areas in a short time period. Results from this study indicate that both remote sensing and GIS data analysis is potential for various applications oriented towards improving the monitoring and control of potential future vector born disease outbreaks.

5. Recommendation

In the current study we highly recommend the use of remote sensing data (e.g. Landsat 8) in the standard procedures of vector control since it has proven to be able to determine the environmental factors and conditions controlling the reproduction and growth of such vectors. Our results can be useful for public health professionals responsible for vector control in Makkah region since the city if vulnerable to be affected by infectious diseases, which can be easily transmitted through such vectors during the Hajj and Umrah seasons.

5. References:

[1]. World health organization (WHO) (2006): Mosquitos and other biting Diptera. Available from: http://www.who.int/water_sanitation_health/resources/vector007to28.pdf (Last accessed on 2018 Feb 5).

[2]. Hopp, M.J. and Foley, J.A., 2001. Global-scale relationships between climate and the dengue fever vector, *Aedes aegypti*. Clim Change 48: 441-463.

[3]. Bliss, A.R. and Gill, J.M., 1993. The effects of freezing on the larvae of Aedes aegypti. Amer J Trop Med Hyg 13: 583-588.

[4]. Center for Disease Control (CDC): Mosquito Life cycle (Aedes aegypti). Available at: https://www.cdc.gov/dengue/resources/factSheets/MosquitoLifecycleFINAL.pdf.

[5]. J ansen, C.C., Beebe, N.W., 2010. The dengue vector *Aedes aegypti*: what comes next. Microbes Infect. 12, 272–279.

[6]. Rowley, W.A., Graham, C.L., 1968. The effect of temperature and relative humidityon the flight performance of female *Aedes aegypti*. J. Insect Physiol. 14,1251–1257.

[7]. Rueda, L.M., Patel, K.J., Axtell, R.C., Stinner, R.E., 1990. Temperature-dependent development and survival rates of *Culex quinquefasciatus* and *Aedes aegypti* (Diptera: Culicidae). J. Med. Entomol. 27, 892–898.

[8]. Kitron U. (1998): Landscape ecology and epidemiology of vector-borne diseases: tools for spatial analysis. J Med Entomol.; 35(4):435-45.

[9]. Kalluri S, Gilruth P, Rogers D, Szczur M (2007): Surveillance of arthropod vector-borne infectious diseases using remote sensing techniques: a review- PLoS pathogens, (3) 10, 1361-1371.

[10]. Roberts DR, Paris JF, Manguin S, Harbach RE, Woodruff R, Rejmankova E, Polanco J, Wullschleger B, Legters LJ. (1996): Predictions of malaria vector distribution in Belize based on multispectral satellite data. Am J Trop Med Hyg.; 54(3):304-8.

[11]. Beck LR, Lobitz BM, Wood BL (2000): Remote sensing and human health: new sensors and new opportunities. Emerging infectious diseases, 6 (3), 217-227.

[12]. Beck LR, Rodriguez MH, Dister SW, Rodriguez AD, Rejmankova E, Ulloa A, Meza RA, Roberts DR, Paris JF, Spanner MA, et al. (1994): Remote sensing as a landscape epidemiologic tool to identify villages at high risk for malaria transmission. Am J Trop Med Hyg.; 51(3):271-80.

[13]. Sithiprasasna R, Lee WJ., Ugsang DM. and Linthicum K. (2005): Identification and characterization of larval and adult anopheline mosquito habitats in the Republic of Korea: potential use of remotely sensed data to estimate mosquito distributions. International Journal of Health geographics, 4-17

[14]. Tuno N, Okeka W, Minakawa N, Takagi M, Yan G (2005): Survivorship of Anopheles gambiae sensu stricto (Diptera: Culicidae) larvae in western Kenya highland forest. J Med Entomol.; 42(3):270-277.

[15]. Mushinzimana, Emmanuel; Munga, Stephen; Minakawa, Noboru; Li, Li; Feng, Chen-chieh; Bian, Ling; Kitron, Uriel; Schmidt, Cindy; Beck, Louisa; Zhou, Guofa; Githeko, Andrew K; Yan, Guiyun (2006): Landscape determinants and remote sensing of anopheline mosquito larval habitats in the western Kenya highlands. Malaria Journal,5:13. doi:10.1186/1475-2875-5-13

[16]. Linthicum KJ, Bailey CL, Davies FG, Tucker CJ. (1987): Detection of Rift Valley fever viral activity in Kenya by satellite remote sensing imagery. Science.; 235(4796):1656-1659.

[17]. Al-Ghamdi, K., Khan M.A., & Mahyoub, J., 2009. Role of climatic factors in the seasonal abundance of Aedes aegypti L. and dengue fever cases in Jeddah province of Saudi Arabia. Curr. World Environ. 4, 307–312.

[18]. Dale PE, Ritchie SA, Territo BM, Morris CD, Muhar A, Kay BH. (1008): An overview of remote sensing and GIS for surveillance of mosquito vector habitats and risk assessment. J Vector Ecol.; 23(1):54-61.

[19]. Hay SI, Tatem AJ, Graham AJ, Goetz SJ (2006): Global environmental data for mapping infectious disease distribution. Advances in Parasitology. 62, 37-77.

[20]. Eisen L and Eisen RJ (2011): Using Geographic Information Systems and Decision Support Systems for the Prediction, Prevention, and Control of Vector-Borne Diseases. Annual Review of Entomology, Vol. 56:41-61

[21]. General Authority for Statistics in Saudi Arabia 2017, Available online at: https://www.stats.gov.sa/en

[22]. WHO. Dengue: guidelines for diagnosis, treatment, prevention and control. Geneva 2009. Available from: http://www.who.int/tdr/publications/documents/dengue-diagnosis.pdf

[23]. S. J. Connor, M. C. Thomson, P. J. Milligan, and S. P. Flasse. 1996. “The ecology of malaria as seen from Erth observation satellites. Annals of Tropical Medicine and Parasitology 90(3): 243-264.

[24]. A. Rajeshwari and N. Mani, “Estimation of land surface temperature of dindigul district using landsat 8 data,” International Journal of Research in Engineering and Technology, vol. 3, no. 5, pp. 122–126, 2014.

[25]. F. Becker and Z.-L. Li, “Towards a local split window method over land surfaces,” International Journal of Remote Sensing, vol. 11, no. 3, pp. 369–393, 1990.

[26]. S. Ustin, Manual of Remote Sensing: Remote Sensing for Natural Resource Management and Environmental Monitoring, John Wiley & Sons, Hoboken, NJ, USA, 2004.

[27]. Using the USGS Landsat 8 Product, Available from: https://landsat.usgs.gov/using-usgs-landsat-8-product (Last accessed on 2018 Jan12).

[28]. H.-Q. Xu and B.-Q. Chen, “Remote sensing of the urban heat island and its changes in Xiamen City of SE China,” Journal of Environmental Sciences, vol. 16, no. 2, pp. 276–281, 2004.

[29]. J. A. Sobrino, J. C. Jiménez-Muñoz, and L. Paolini, “Land surface temperature retrieval from LANDSAT TM 5,” Remote Sensing of Environment, vol. 90, no. 4, pp. 434–440, 2004.

[30]. J. C. Jimenez-Munoz, J. A. Sobrino, A. Gillespie, D. Sabol, and W. T. Gustafson, “Improved land surface emissivities over agricultural areas using ASTER NDVI,” Remote Sensing of Environment, vol. 103, no. 4, pp. 474–487, 2006.

[31]. M. Stathopoulou and C. Cartalis, “Daytime urban heat islands from Landsat ETM+ and Corine land cover data: an application to major cities in Greece,” Solar Energy, vol. 81, no. 3, pp. 358–368, 2007. View at Publisher ·

[32]. M. Stathopoulou and C. Cartalis, “Daytime urban heat islands from Landsat ETM+ and Corine land cover data: an application to major cities in Greece,” Solar Energy, vol. 81, no. 3, pp. 358–368, 2007.

[33]. Q. H. Weng, D. S. Lu, and J. Schubring, “Estimation of land surface temperature-vegetation abundance relationship for urban heat island studies,” Remote Sensing of Environment, vol. 89, no. 4, pp. 467–483, 2004.

[34]. (Pettorelli et al., 2005): Pettorelli, N., Vik, J.O., Mysterud, A., Gaillard, J.M., Tucker, C. J. & Stenseth, N.C., (2005), Using the satellite-derived NDVI to assess ecological responses to environmental change, Trends in ecology & evolution,20(9), pp. 503-510.